Surface Discharge Effects

K. G. Balmain

Reprinted from **Space Systems and Their Interactions with Earth's Space Environment**, *edited by Henry B. Garrett and Charles P. Pike, Vol. 71 of Progress in Astronautics and Aeronautics.*

SURFACE DISCHARGE EFFECTS

K.G. Balmain*
University of Toronto, Toronto, Canada

Abstract

Specimens of Mylar sheet were exposed to a 20-kV electron beam. The resulting surface discharge arcs were photographed, and the discharge current into a metal backing plate was measured as a function of time. Discharge damage tracks were photographed using a scanning electron microscope and a light microscope. The area of the Mylar sheet was defined by a round aperture in a close-fitting metal mask, and the current pulse characteristics were plotted against area on log-log paper. The plots appear as straight lines (due to power-law behavior) with slopes of 0.50 for the peak current, 1.00 for the charge released, 1.50 for the energy dissipated, and 0.53 for the pulse duration.

Introduction

Arc discharges on thin sheets of spacecraft dielectric material have been discussed at length in the published proceedings of various conferences[1-4] and in review papers.[5-7] These discharges have been given names such as "punchthrough," "blowoff," and "flashover," all very vivid in keeping with their strength, dramatic appearance, and destructiveness. To date, direct measurements in space of discharge properties have been few,[8,9] so almost all of the direct observations and measurements have been done in laboratory vacuum chambers in which 10- to 30-keV electrons at current densities of the order of 10 nA/cm^2 have been directed at the insulating materials under test. Exposure to these electrons produced sporadic lightning-like arcs across the dielectric surface,[10] the arcs having a spider-web or feathery appearance, sometimes seeming to emanate from a very bright spot. These bright focal points often occurred near the edge of the material or were associated with

Presented in part at the 1978 USAF/NASA Spacecraft Charging Technology Conference, Colorado Springs, Colo., Oct. 31-Nov. 2, 1978. Copyright © American Institute of Aeronautics and Astronautics, Inc., 1979. All rights reserved.

*Professor, Department of Electrical Engineering.

punctures through the material. In general, each discharge arc produced a strong, short pulse of current into the metal surface underlying the dielectric sheet.

Earlier work by Gross[11,12] showed that a dielectric block irradiated with 2-MeV electrons could retain its charge for a long period, releasing it in an arc discharge stimulated by the insertion of a grounded needle. The resulting damage tracks were concentrated at the stopping distance of the 2-MeV electrons. Meulenberg[13] showed that breakdown-level electric fields could develop between the embedded layer of electrons and the dielectric surface which could be somewhat positive as a result of secondary emission. Therefore, breakdown could occur from the embedded electrons either to the surface (blow-off) or to the underlying metal substrate (punchthrough) depending on the circumstances. Such initial breakdown at a specific point could then be followed by an arc discharge propagating through the layer of embedded charge (flashover), as suggested by the damage tracks observed by Gross. Discharge propagation thus could provide the mechanism for mobilizing charge in sufficient quantity to produce the phenomenon of charge "cleanoff" observed by many laboratory experimenters.

Most laboratory experiments to date have involved dielectric areas much smaller than the exposed dielectric areas existing on operational synchronous-orbit satellites, so the question of area scaling of charge/discharge phenomena arises naturally. Certainly it is easier and faster to carry out

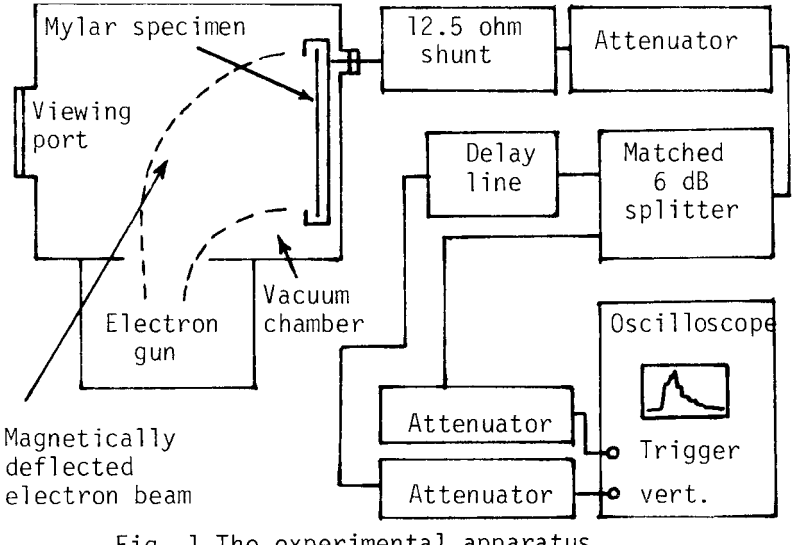

Fig. 1 The experimental apparatus.

small-scale experiments, compared with large-scale experiments in vacuum chambers large enough to hold spacecraft components or even an entire spacecraft.

It has been shown[14] that, for surface discharges on metal-backed polymer dielectrics, the peak discharge current is proportional to the surface area raised to a power "p" lying between 0.5 and 0.8 for the range of areas between 0.2 cm^2 and 20 cm^2. The most consistent results shown were for Teflon with a value of $p = 0.58$, whereas the results from Mylar gave $p = 0.76$ with more scatter in the plotted points. In the foregoing experiments the dielectric surface area was determined by cutting the test specimen to size in the shape of either a square or a rectangle with a 2:1 side length ratio. It is also possible to define the effective charged area by controlling the size of the incident electron beam,[14] a procedure which can give charged areas in the range of 10^{-5} cm^2 to 10^{-3} cm^2, along with peak discharge currents which for Teflon lie approximately on the line with slope $p = 0.58$ referred to above, extrapolated downward from much larger areas.

Cutting a dielectric specimen to size means that the stressed and perhaps damaged edges are exposed to the electron beam. Furthermore, the edges adjacent to the grounded metal substrate in most experiments, receive a progressively larger

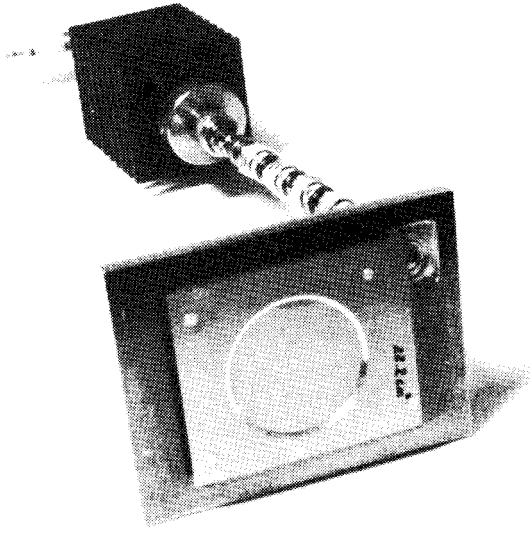

Fig. 2 The specimen mounting assembly with circular-aperture aluminum mask. The four 50-ohm shunts and the first attenuator are attached to the coaxial feed-through receptacle.

electron flux as the incident electron beam is deflected away from the accumulating charge in the mid-region of the specimen. Clearly a better means of defining the effective charged area is required, one such means being the metal mask technique described below.

Experiment Design

The vacuum chamber and electrical instrumentation are shown in Fig. 1. A vacuum-sealed bulkhead receptacle carries the discharge pulse signal to a 10-ohm termination consisting of four 50-ohm coaxial feed-through terminations (comprising a 12.5-ohm shunt) plus the 50-ohm input to the attenuator and measurement cable. The attenuators, splitter, and delay line are all matched and calibrated up to 4 GHz. All cables are matched at both ends to prevent ringing. The oscilloscope has a 400-MHz bandwidth. Precautions were taken to insure adequate shielding of operating personnel from X-radiation.

Figures 2 and 3 show the specimen mounting plate and a typical circular-aperture metal mask used to define the charged area on the specimen surface. For each such area the experimental procedure was to set the incident 20-keV electron beam to a current density which produced approximately one discharge every 15 sec. For the largest areas this resulted in a current density of about 100 nA/cm^2 and for the smallest areas about 10 $\mu A/cm^2$; variation of the current density over this range

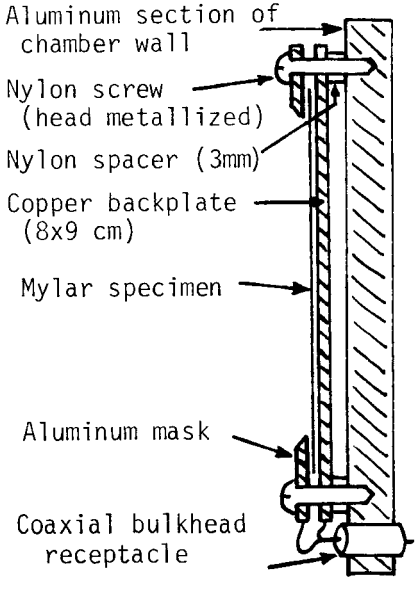

Fig. 3 Details of the specimen mounting assembly.

affected only the discharge rate and had no noticeable effect on the amplitude or shape of the discharge current pulses for the 125-μm thick Mylar specimens under test.

Phenomena Expected

Figure 4 shows the expected effects of exposing a dielectric sheet to a monenergetic beam of electrons. First, the 20-keV electrons penetrate to the stopping depth, estimated to be 7 to 8 μm. As the embedded charge builds up, the electron energy upon impact is reduced, resulting in somewhat shallower deposition.[15] The accumulated electrons induce positive charge in the underlying metal substrate and in the nearby edge of the metal mask, and the incident beam is deflected by electrostatic forces to deposit the highest charge concentration close to the mask edge.

Relatively thin specimens or specimens with edges shielded against the incident electron beam have a tendency to discharge from the embedded electron layer through to the substrate via the "punchthrough" arc[16] indicated as "a" in Fig. 4. In cases

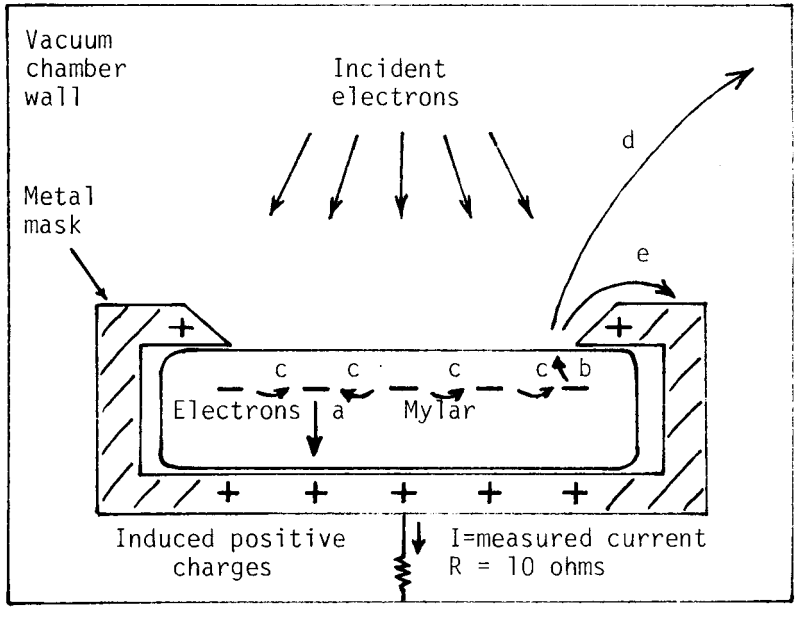

Fig. 4 Illustration of possible charging and discharging phenomena. a) punchthrough arc, b) blowoff arc (arc to surface), c) flashover arc (propagating subsurface discharge), d) ejected electrons going to chamber wall, and e) ejected electrons going to mask.

where there is a high near-surface field and especially close to an edge, an arc through to the surface ("b") or "blowoff" arc will occur, accompanied by a strong ejection of electrons. This will leave behind a high-field region inside the dielectric, resulting in a propagating "flashover" arc "c" through the layer of embedded electrons. Depending on the circumstances, the flashover may produce sporadic or continuous blowoff of material as it propagates.

The punchthrough arc is sufficiently energetic when it occurs to leave a puncture all the way through the dielectric specimen. The incident electrons would see this hole as a grounded spot and would tend to focus on it so that the punchthrough hole would then become the focal point for subsequent discharge activity in the form of flashover arcs and blowoff arcs.

The discharge current measurement consists of measuring the voltage across the resistor R in Fig. 4. It is very important to note that the only discharge currents measured by this method are those arising from the ejected-electron orbits "d" which terminate on the chamber walls. Electron orbits "e" terminating on the mask or punchthrough arcs will not result directly in the flow of current through R.

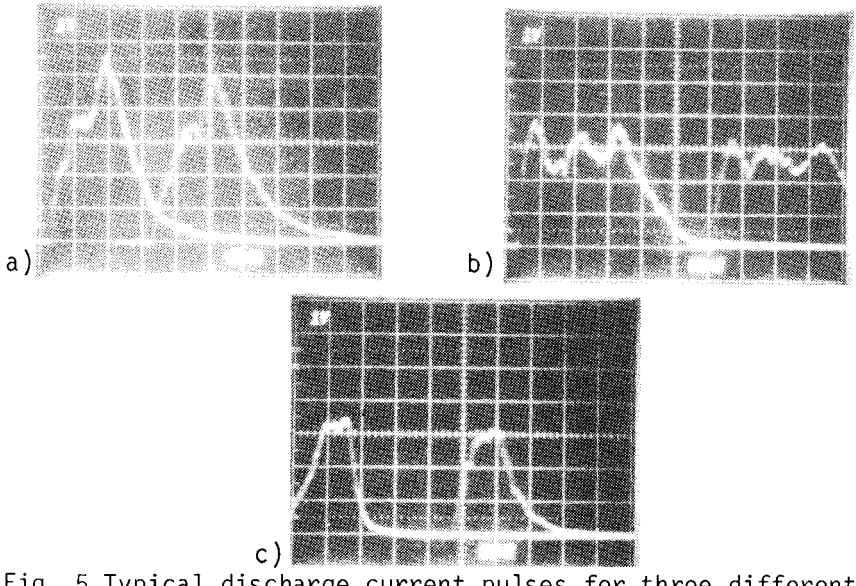

Fig. 5 Typical discharge current pulses for three different Mylar specimens. a) Area = 22.2 cm^2, I_m = 44.5 A and 39.7 A. b) Area = 22.2 cm^2, I_m = 30.2 A (see Fig. 7 for photograph of arc), and I_m 26.2A. c) Area = 47.6 cm^2, I_m = 110.7 A and 101.2 A.

The Arc Discharges

The measured discharge current pulses of Fig. 5 provide some idea of the normal range of pulse shapes encountered. For each setup (all experimental conditions fixed) it was quite common to measure 5 to 10 current pulses of nearly identical shapes, as suggested by the nearly identical pairs in Fig. 5. The shortest pulses measured (for small dielectric areas, not shown) exhibited a small degree of negative overshoot and ringing, possibly because their rise and fall times were close to the limit for the oscilloscope used.

Visual inspection of the discharge arcs revealed that no two arc patterns are identical although there may be a degree of similarity and a few common bright-spot focal points in a given setup, especially near the mask edge. Typical discharge arcs are shown in Figs. 6-9.

Discharge Damage

In view of the maximum electron penetration distance of about 8 μm, one might expect to see damage down to approximately this depth. In the search for this damage, a specimen was selected for which progressively increasing mask diameters had been used and on which approximately 15 discharges per mask had

Fig. 6 Arc showing simultaneous edge streamers. Mylar area = 22.2 cm^2.

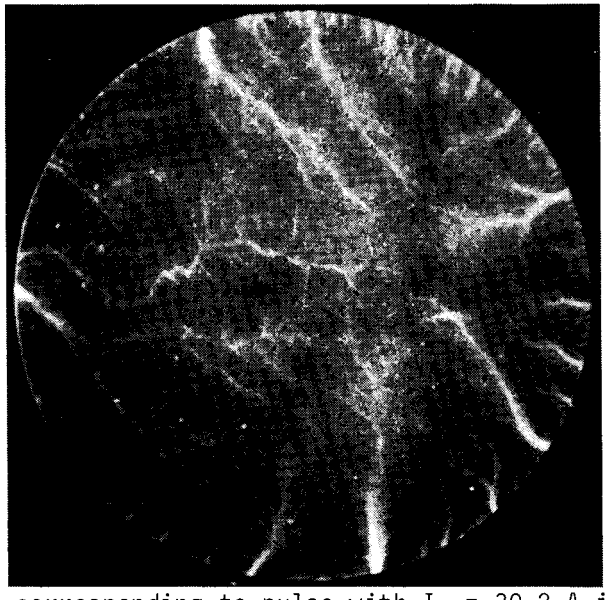

Fig. 7 Arc corresponding to pulse with I_m = 30.2 A in Fig. 5. Mylar area = 22.2 cm^2.

Fig. 8 Arc with single primary streamer. Mylar area = 47.6 cm^2. Two light shaded regions are the result of electron-impact luminescence during an unusually long open-shutter period before the discharge.

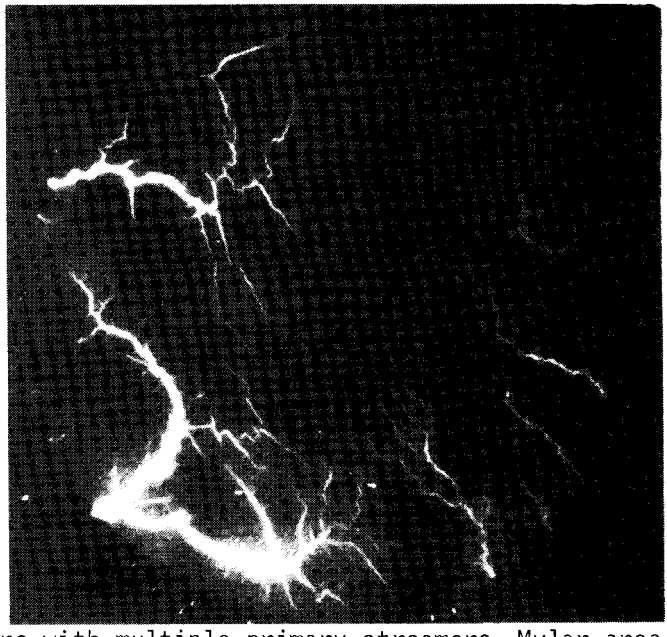

Fig. 9 Arc with multiple primary streamers. Mylar area = 47.6 cm^2.

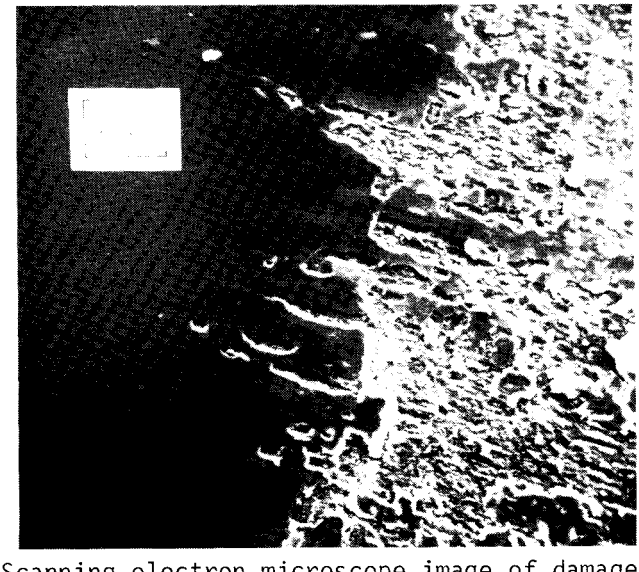

Fig. 10 Scanning electron microscope image of damage along one of the mask-edge lines on a single specimen for which a sequence of progressively larger mask apertures had been used.

Fig. 11 Scanning electron microscope image: magnification of Fig. 10.

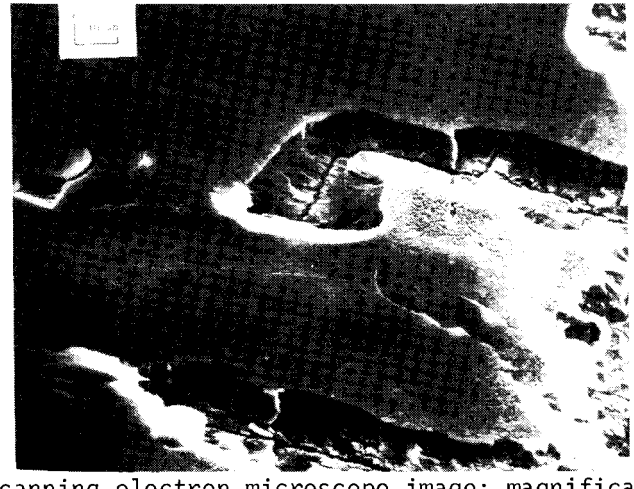

Fig. 12 Scanning electron microscope image: magnification of Fig. 11.

occurred. The specimen was vacuum-coated with gold and viewed in a scanning electron microscope. The resulting micrograph (Fig. 10) clearly shows two regions of greatly differing damage separated by one of the lines along which the mask edge had been positioned.

Micrographs of increasing magnification are shown in Figs. 11-14, in which it is clear that the most characteristic damage consists of a deep channel of less than 1 μm in width at the bottom of a much wider depression whose surface apparently was blown off by the force of the discharge arcs. Also visible, especially near the top of Fig. 14, are two apparent holes in the side of the depression.

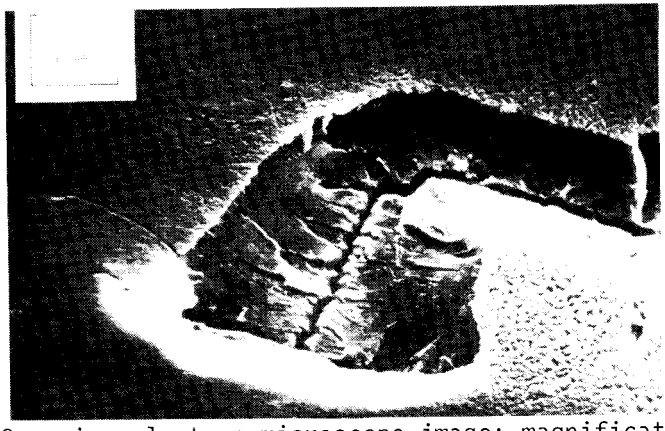

Fig. 13 Scanning electron microscope image: magnification of Fig. 12.

Fig. 14 Scanning electron microscope image: magnification of Fig. 13. Note two tunnel openings near top of page.

Transmitted-light microscope photographs also were taken and are shown in Figs. 15-17. These reveal a network of damage tracks underlying the relatively undamaged portion of the surface. Two of these damage tracks open out into the two holes already mentioned with respect to Fig. 14. It therefore appears that the subsurface damage tracks are tunnels along which the discharge arcs are channeled, sometimes blowing off the top few microns of the material surface. The tunnel radii appear to be approximately 0.3 μm, and the tunnel depths appear to be mostly 4 to 8 μm below the surface.

It is worth noting that complete puncture of the specimen (or punchthrough) was extremely rare in these experiments on

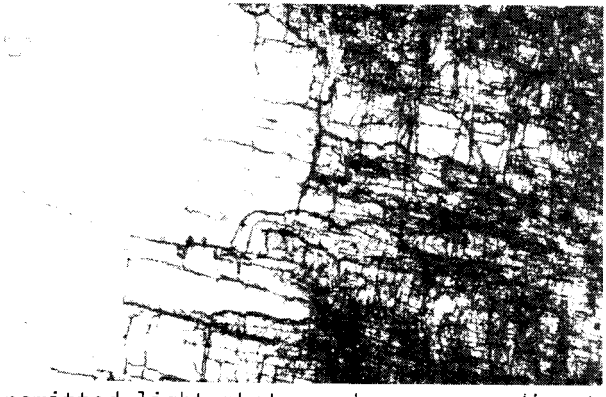

Fig. 15 Transmitted-light photograph corresponding to Fig. 11.

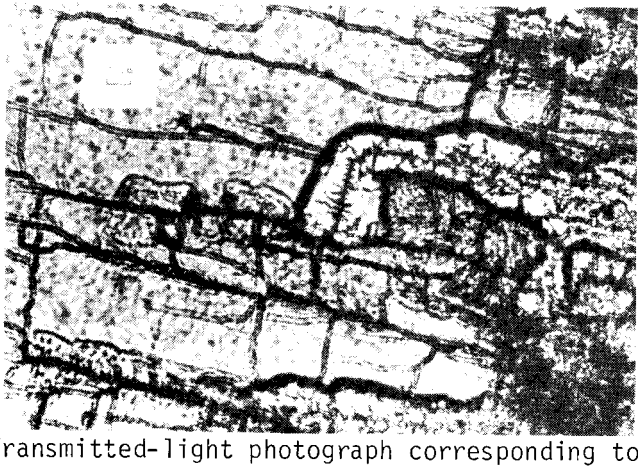

Fig. 16 Transmitted-light photograph corresponding to Fig. 12.

125-μm thick Mylar. In fact, it occurred in only one sequence of experiments involving the use of progressively larger masks on a single specimen.

Area Scaling

A sequence of experiments was carried out using the full range of mask diameters available and using a new, unexposed specimen for each mask size. The peak currents I_m are plotted in Fig. 18 against specimen area, and each averaged point is accompanied by a vertical bar indicating the full range of currents used to calculate the average. The straight line drawn through the larger-area points has a slope of 0.50, indicating that the peak currents are proportional to the square root of the area - that is, proportional to the linear dimensions of

Fig. 17 Transmitted-light photograph corresponding to Fig. 13.

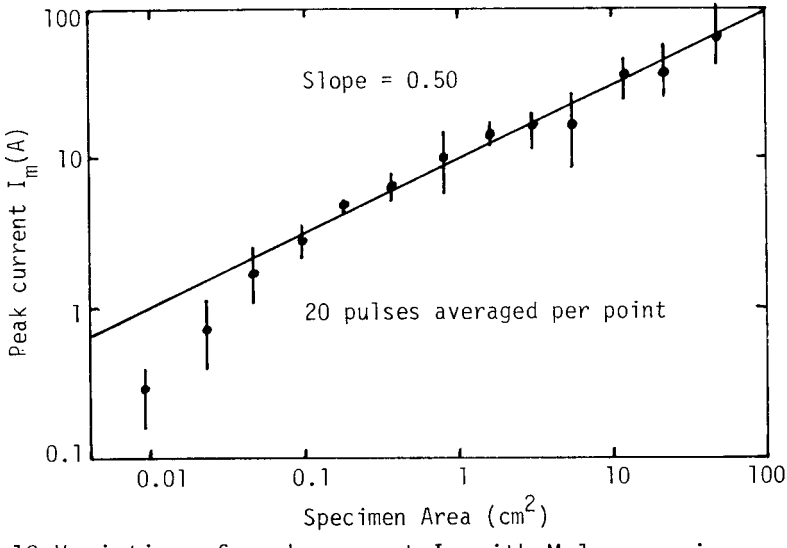

Fig. 18 Variation of peak current I_m with Mylar specimen area, a different unexposed specimen being used with each mask aperture size.

the aperture. It is worth noting that this straight line extrapolates to $I_m \approx 1000$ A at an area of 1 m^2.

The charge Q passing through the measurement system is given by

$$Q = \int I \, dt$$

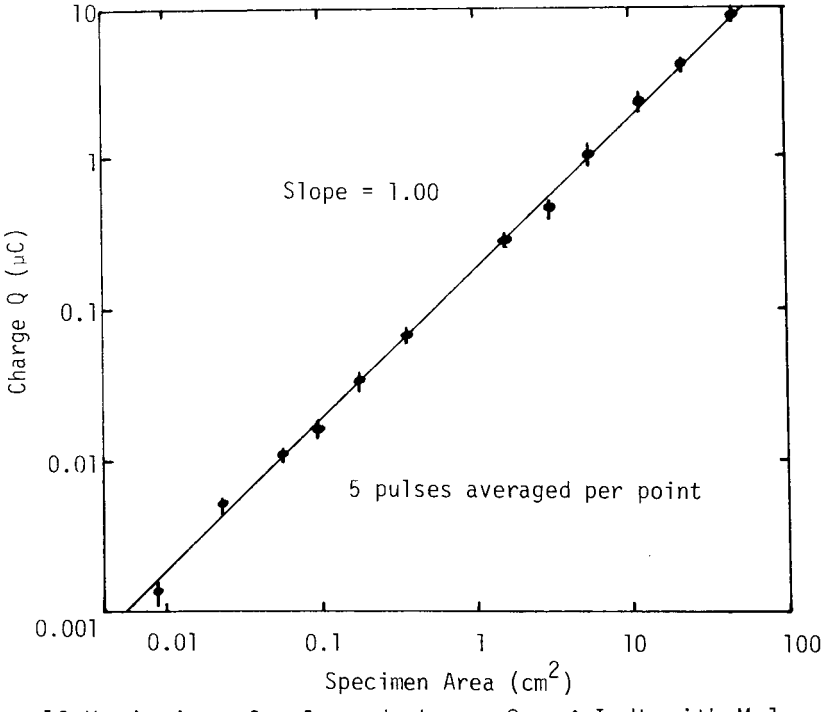

Fig. 19 Variation of released charge $Q = \int I\,dt$ with Mylar specimen area for the same conditions as in Fig. 18.

an integration which was carried out using data from oscilloscope photographs. The results of these computations are shown in Fig. 19 which includes a straight-line approximation having a slope of 1.00 indicating charge proportionality to specimen area.

The energy dissipated in the load resistor R is given by

$$E = R \int I^2\,dt$$

and the resulting graph of energy against area is shown in Fig. 20. The highest energy point plotted on the graph is 5 mJ; this is sufficient to burn out a typical 50-ohm coaxial microwave attenuator rated at 20 W average, a lesson which was learned by experience during the early stages of the research program!

The pulse duration was calculated from the relation

$$T = \frac{1}{I_m} \int I\,dt$$

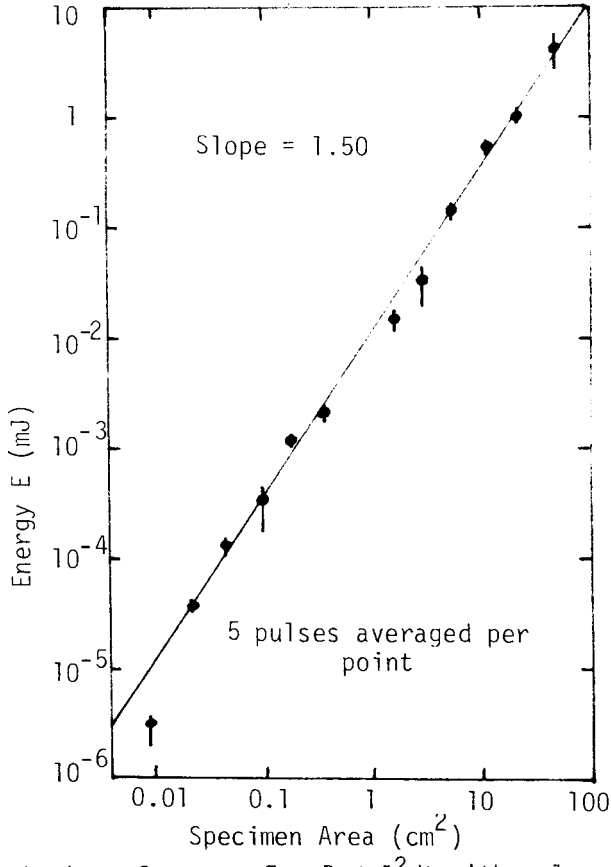

Fig. 20 Variation of energy $E = R \int I^2 dt$ with mylar specimen area. The energy is dissipated in a load resistor R = 10 ohms. The conditions are the same as in Fig.18.

and the resulting graph of duration against area is shown in Fig. 21. The straight-line approximation has a slope of 0.53 although one would have expected a slope of 0.50 because the duration calculated in this way is just the ratio of released charge to peak current. Departure from the straight-line approximation is noticeable for small areas and thus for short pulses, this departure taking the form of extended pulse durations and reduced peak currents as well. The probable cause of this effect is the 400-MHz bandwidth of the oscilloscope.

Figure 21 also can be used to estimate the propagation velocity of the flashover arc, assuming that the pulse duration is determined by the propagation time of an arc across the

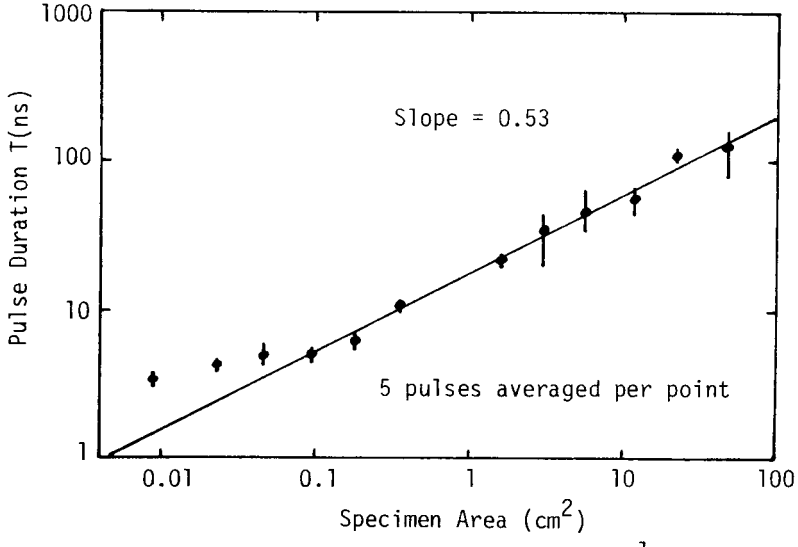

Fig. 21 The variation of pulse duration $T = I_m^{-1} \int I\,dt$ with Mylar specimen area for the same conditions as in Fig. 18.

specimen. From the graph, an aperture radius of 1 cm corresponds to a pulse duration of 33 nsec, the ratio giving a velocity of 3×10^5 m/sec.

In order to assess cumulative arc effects, an experimental sequence was carried out using progressively increasing mask sizes on the same Mylar specimen. As already indicated, this experiment produced occasional punchthroughs, and also this specimen was used for the damage photographs already discussed. In spite of the differences in procedure and damage, the resulting peak current graph of Fig. 22 is essentially indistinguishable from the graph of Fig. 18 for experiments employing unexposed specimens for each area. This similarity may be due to the fact that the results of Fig. 22 are for specimens having an unexposed annular ring of dielectric adjacent to the mask edge for each new, larger area in the experimental sequence.

The reverse sequence also was tried, involving progressively decreasing mask areas. The peak current, released charge, energy dissipated, and pulse duration are graphed as functions of area in Figs. 23-26. Material fatigue was most evident at the smallest areas. In these cases one or two discharges occurred immediately after the electron beam was turned on, followed by a complete absence of discharges, so that no data was recorded. Apart from this there is little difference

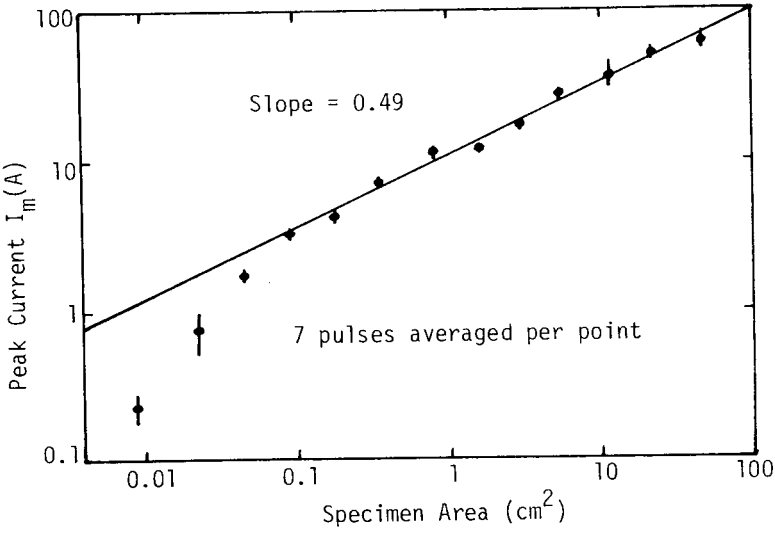

Fig. 22 Peak current I_m for an experimental sequence in which a single specimen was used with progressively increasing mask aperture diameters.

in comparison with the cases discussed previously, the difference amounting to a slight decrease in peak current and a slight increase in pulse duration.

Interpretation

The proportionality of the released charge to the specimen area is demonstrated in Fig. 19 in which the plotted points exhibit little scatter and little departure from exact proportionality even for the smallest areas tested. This suggests that a constant fraction of the charge incident on any given area discharges via electron orbits going to the chamber wall. Now suppose that a fraction of the charge discharges via electron orbits going directly to the metal mask ("e" in Fig. 4). However, the outside dimensions of the mask are constant, so the exposed mask area increases as the exposed dielectric area decreases. Therefore, one might expect that an increasing fraction of the ejected electrons would go to the mask as the dielectric specimen area is decreased, leaving a smaller fraction for the current to the walls. This apparently does not happen, according to Fig. 19, so that the discharge current going to the mask is most probably negligible.

If the discharge were similar to the discharge of a capacitor through a resistor connected across the capacitor termin-

als, then the peak current would be proportional to the incident beam energy (capacitor voltage), which is constant, but independent of specimen area (capacitance). Also, the energy dissipated in the resistor would be proportional to area. Neither of these proportionalities applies to the surface discharges, so the discharge mechanism is not similar to that of a capacitor.

The appearance of the discharge arcs and the arc damage suggests that the discharge must propagate at a finite velocity. One such finite-velocity mechanism is the electron-hopping mechanism suggested by Inouye and Sellen.[17] Leadon and Wilkenfeld[18] also have estimated the inductance and capacitance of the discharge arc to calculate the discharge time duration. Regardless of the precise mechanism involved, suppose that a discharge initiates at a point and expands outward uniformly at a constant velocity. If the ejected electrons emerge from the wave front, then the discharge current would be proportional to the length of the wave front. The maximum wave front length would be controlled by the linear dimensions of the exposed dielectric, so the peak current would be proportional to the square root of the specimen area, exactly as observed. The pulse duration also would have the same proportionality, approx-

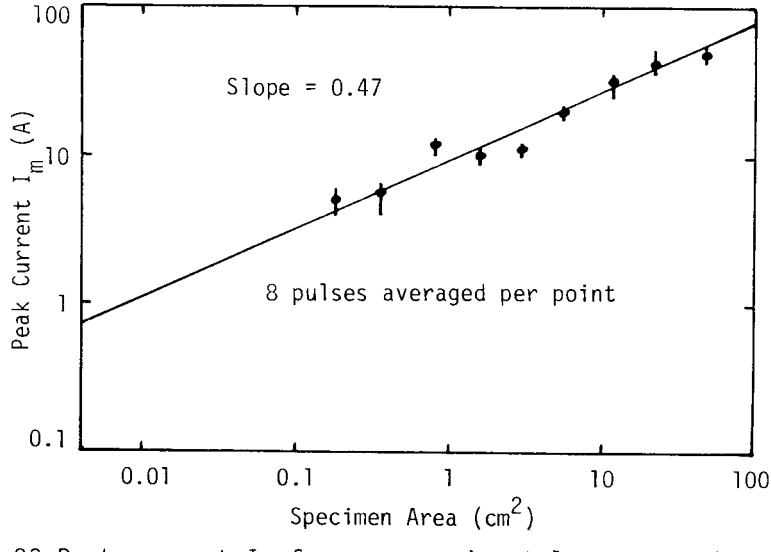

Fig. 23 Peak current I_m for an experimental sequence in which a single specimen was used with progressively decreasing mask aperture diameters.

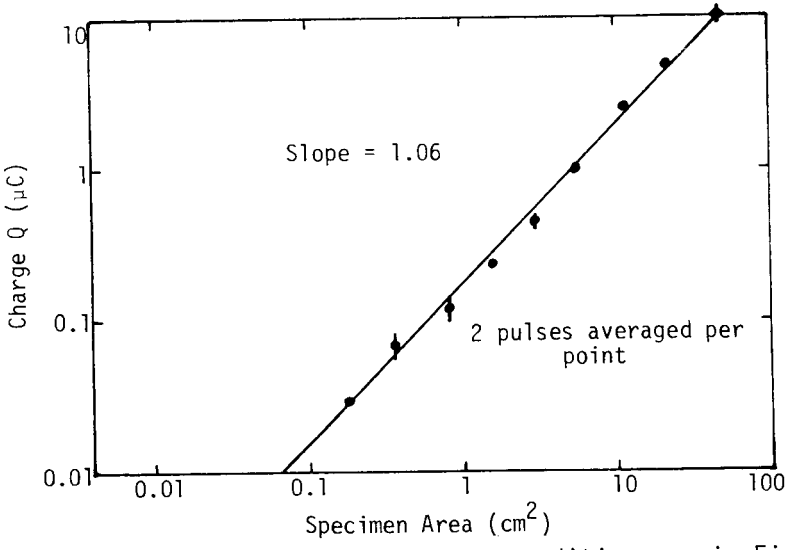

Fig. 24 Released charge Q for the same conditions as in Fig.23.

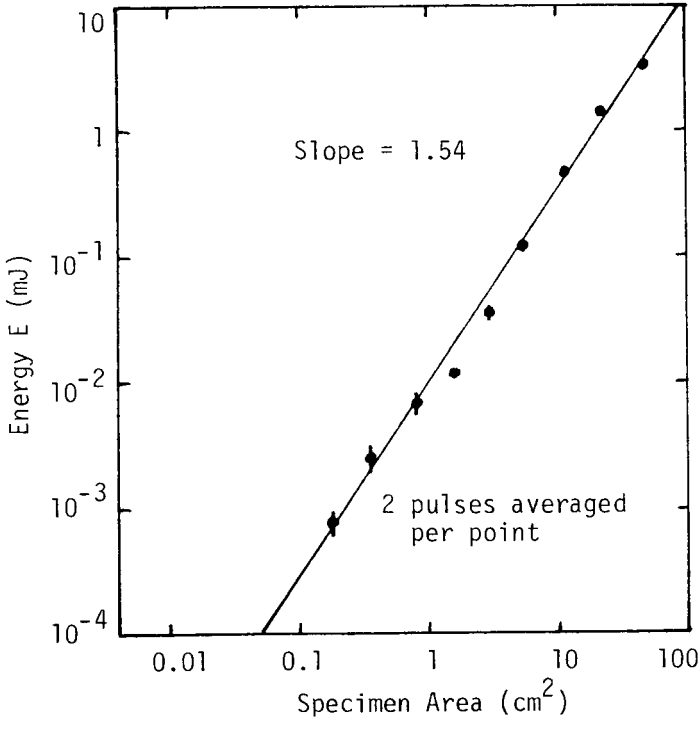

Fig. 25 Energy dissipated E for the same conditions as in Fig.23.

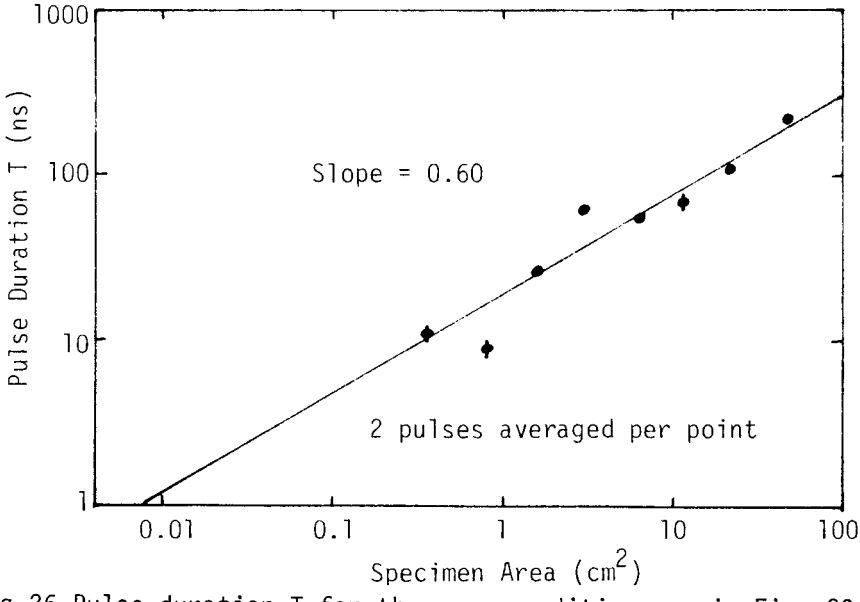

Fig 26 Pulse duration T for the same conditions as in Fig. 23.

imately as observed. A sequence of linear, branching discharge paths should produce the same result overall.

If the discharge propagation were entirely subsurface and all electron ejection from the point of initiation, then the process would involve two velocities. These would be the velocity of the discharge wave front and the velocity of subsurface electron propulsion toward the point of ejection. Thus the apparent velocity deduced from measured currents would in fact be the sum of these two velocities.

A vivid analogy is that of a "flash flood" caused by a sudden, heavy rainstorm over a specified area. If the water runoff velocity were constant, then the peak runoff water flow would be proportional to the square root of the storm area, and the runoff duration would have the same proportionality.

Conclusions

Surface discharge arcs on metal-backed Mylar exhibit electrical characteristics which scale with variations in specimen area according to well-defined power laws. The characteristics identified are peak current, released charge, energy dissipated, and pulse duration, and the respective powers are 0.50, 1.00, 1.50, and 0.53.

The discharge arcs appear to be channeled into hair-like branching tunnels at the penetration depth, with occasional blowoffs of surface material. These tunnels do not cover the entire surface, however, so there remains an open question as to the discharge mechanism between the tunnels. There are signs of material fatigue in the electrical measurements of discharge properties, but these indications of fatigue seem small in view of the very extensive surface damage visible in the scanning electron microscope, especially near the mask edge.

The surface discharges appear to propagate at a well-defined velocity of about 3×10^5 m/sec. Propagation at a constant velocity is consistent with the experimental observations of the area scaling laws for peak current and pulse duration.

In considering the application of these results to materials on synchronous-orbit spacecraft, there are several differences between the laboratory conditions and the conditions in space which should be kept in mind. In the laboratory, the incident electron fluxes used were much higher than those encountered in space, the higher fluxes having been employed in order to have a high enough discharge rate for reasonably rapid accumulation of data and in order to have reasonably predictable discharge occurrence times for high-quality arc photography. Even though electrical independence of electron flux was noted in the flux range employed, there does exist the possibility of different behaviour at much lower fluxes. In addition, unlike the situation in space, the laboratory experiments involved monoenergetic electrons normally incident on the dielectric, with no incident ions and no ambient plasma. As for the various types of materials used on spacecraft, previous work[14] has suggested that different types of polymers have much in common with respect to discharge properties, so it is possible that the results of this study will apply approximately to other highly insulating polymers.

Overall, the most remarkable result of this experimental study is that, in spite of the variability in discharge arc appearance from one arc to the next, in spite of extensive damage inflicted on the dielectric surface, and in spite of the obvious complexity of the detailed discharge process, there still exists a high degree of order in the electrical properties of the current pulses observed. This degree of order strongly suggests the existence of a set of well-defined physical principles governing the behavior of surface discharges and underlines the importance of seeking out these principles.

Acknowledgments

The research was supported by the Natural Sciences and Engineering Research Council of Canada under Grant No. A-4140. The experiments and data reduction were carried out by G.R. Dubois, whose contributions are gratefully acknowledged.

References

[1]Rosen, A., ed., Progress in Astronautics and Aeronautics: Spacecraft Charging by Magnetospheric Plasmas, Vol. 47, AIAA, New York, 1976.

[2]Pike, C.P. and Lovell, R.R., eds., Proceedings of the Spacecraft Charging Technology Conference, Rept. AFGL-TR-77-0051/ NASA TMX-73537, Feb. 24, 1977.

[3]Goodman, J.M, ed., Effect of the Ionosphere on Space and Terrestrial Systems, Proceedings of an NRL/ONR - sponsored conference, Arlington, Va., January 24-26, 1978, U.S. Government Printing Office Stock No. 008-051-00069-1.

[4]Proceedings of the 1978 USAF/NASA Spacecraft Charging Technology Conference, Colorado Springs, Colo., Oct. 31-Nov. 2, 1978.

[5]Rosen, A., "Large Discharges and Arcs on Spacecraft," Astronautics & Aeronautics, Vol. 13, June 1975, pp. 36-44.

[6]Rosen, A., "Spacecraft Charging: Environment - Induced Anomalies," Journal of Spacecraft and Rockets, Vol. 13, March 1976, pp. 129-136.

[7]Rosen, A., "Spacecraft Charging by Magnetospheric Plasmas," IEEE Transactions of Nuclear Science, Vol. NS-23, Dec. 1976, pp. 1762-1768.

[8]Nanevicz, J.E., and Adamo, R.C., "Transient Response Measurements on a Satellite System," Ref. 2, pp. 723-734.

[9]Shaw, R.R., "Electrical Interference to Satellite Subsystems Resulting from Spacecraft Charging," Ref. 3, pp. 337-345.

[10]Stevens, N.J., Berkopek, F.D., Staskus, J.V., Blech, R.A., and Narciso, S.J., "Testing of Typical Spacecraft Materials in a Simulated Substorm Environment," Ref. 2, pp. 431-457.

[11]Gross, B., "Irradiation Effects in Borosilicate Glass," The Physical Review, Vol. 107, July 15, 1957, pp. 368-373.

[12]Gross, B., "Irradiation Effects in Plexiglas," Journal of Polymer Science, Vol. 27, 1958, pp. 135-143.

[13]Meulenberg, A., "Evidence for a New Discharge Mechanism for Dielectrics in a Plasma," Ref. 1, pp. 237-246.

[14]Balmain, K.G., Kremer, P.C., and Cuchanski, M., "Charged-Area Effects on Spacecraft Dielectric Arc Discharges," Ref. 3, pp. 302-308.

[15]Beers, B.L., Hwang, H.-C., Lin, D.L., and Pine, V.W., "Electron Transport Model of Dielectric Charging," Ref. 4, pp. 209-238.

[16]Yadlowsky, E.J., Hazelton, R.C., and Churchill, R.J., "Characterization of Electrical Discharges on Teflon Dielectrics Used as Spacecraft Thermal Control Surfaces," Ref. 4, pp. 632-645.

[17]Inouye, G.T. and Sellen, J.M., "A Proposed Mechanism for the Initiation and Propagation of Dielectric Surface Discharges," Ref. 3, pp. 309-312.

[18]Leadon, R. and Wilkenfeld, J., "Model for Breakdown Process in Dielectric Discharges," Ref. 4, pp. 704-710.